

Synthesis and study of ScN thin films

Susmita Chowdhury,¹ Rachana Gupta,¹ Parasmani Rajput,² Akhil Tayal,³ Dheemahi Rao,^{4,5,6} Reddy Sekhar,⁷ Shashi Prakash,¹ Ramaseshan Rajagopalan,⁷ S. N. Jha,² Bivas Saha,^{4,5,6} and Mukul Gupta^{8,*}

¹Applied Science Department, Institute of Engineering and Technology, DAVV, Indore, 452017, India

²Beamline Development and Application Section, Physics Group,

Bhabha Atomic Research Centre, Mumbai 400085, India

³Deutsches Elektronen-Synchrotron DESY, Notkestrasse 85, D-22607 Hamburg, Germany

⁴Chemistry and Physics of Materials Unit, Jawaharlal Nehru Centre for Advanced Scientific Research, Bengaluru 560064, India

⁵International Centre for Materials Science, Jawaharlal Nehru Centre for Advanced Scientific Research, Bengaluru 560064, India

⁶School of Advanced Materials (SAMat), Jawaharlal Nehru Centre for Advanced Scientific Research, Bengaluru 560064, India

⁷Surface and Nanoscience Division, Materials Science Group,

Indira Gandhi Centre for Atomic Research, HBNI, Kalpakkam - 603102, India

⁸UGC-DAE Consortium for Scientific Research, University Campus, Khandwa Road, Indore-452 001, India

(Dated: April 18, 2022)

To contemplate an alternative approach for the minimization of diffusion at high temperature depositions, present findings impart viability of room-temperature deposited reactively sputtered ScN thin film samples. The adopted room temperature route endows precise control over the R_{N_2} flow for a methodical structural phase evolution from Sc \rightarrow ScN and probe the correlated physical aspects of the highly textured ScN samples. In the nitrided regime i.e. at $R_{N_2} = 2.5 - 100\%$ flow, incorporation of unintentional oxygen defects were evidenced from surface sensitive soft x-ray absorption spectroscopy study, though less compared to their metal ($R_{N_2} = 0\%$) and interstitial ($R_{N_2} = 1.6\%$) counterparts, due to higher Gibb's free energy for Sc-O-N formation with no trace of ligand field splitting around the O K-edge spectra. To eradicate the sceptism of appearance of N K-edge (401.6 eV) and Sc L-edge (402.2 eV) absorption spectra adjacent to each other, the nascent Sc K-edge study has been adopted for the first time to validate complementary insight on the metrical parameters of the Sc-N system taken into consideration. Optical bandgaps of the polycrystalline ScN thin film samples were found to vary between 2.25 - 2.62 eV as obtained from the UV-Vis spectroscopy, whereas, the nano-indentation hardness and modulus of the as-deposited samples lie between 15 - 34 GPa and 152 - 476 GPa, respectively following a linearly increasing trend of resistance to plastic deformations. Besides, contrary to other early 3d transition metal nitrides (TiN, VN, CrN), a comprehensive comparison of noticeably large homogeneity range in Sc-N has been outlined to apprehend the minuscule lattice expansion over the large R_{N_2} realm.

I. INTRODUCTION

Early 3d transition metal nitrides (TMNs) e.g. ScN, TiN, VN and CrN even though crystallizes in cubic rocksalt-type B1 structure, but distinct band structure manifests heterogeneous electrical conductivity within the family of early TMNs [1, 2]. Among them, ScN as a semiconductor sought a profound research attention in recent times, whereas, the rest of the early 3d TMNs exhibit metallic nature and are substantially well explored since decades [2, 3]. Apart from ScN been a pre-eminent refractory compound (melting point exceeding ≈ 2873 K, corrosion resistant, high hardness of ≈ 21 GPa) [3] exhibiting high thermoelectric *figure-of-merit* (0.3 at 800 K) [4] and assist as a template for the growth of low dislocation density GaN [5], ScN further possess immense functionalities in conjunction with other TMNs viz. Sc_xGa_{1-x}N as light emitting diodes [6], Al_{1-x}Sc_xN as MEMS magnetoelectric sensors [7, 8], epitaxial (Zr,W)N/ScN - metal/semiconductor superlattices as thermionic energy conversion devices [9] etc. Besides

these intriguing aspects, the lowest enthalpy of formation ($\Delta H_f^0 = -19.79$ eV) [10] Sc-O of Sc compared to other TMNs is the principal intricacy for synthesis of pure ScN, resultant being an unintentional n-type degenerate semiconductor [11, 12].

Hence for application based perspectives, to modulate the band structure engineering for superior device performances, so far, most of the studies adopted high vacuum ($\leq 10^{-8}$ Torr) depositions to ensure low defect concentrations with atomically smooth epitaxial growth of ScN thin film samples on variety of single crystal substrates (MgO, Al₂O₃, GaN, SiC etc.) [13-16], and few of them aided with process parameters are tabulated in Table I. As can be seen from Table I, conventional use of high substrate temperature ($T_s \geq 823$ K) has been an integral part during the synthesis of ScN thin film samples, possibly due to higher adatom mobility promoting enhanced crystalline defect free ScN growth [17]. In addition, intensive research attention have also been dedicated to get an insight on explicit defect contributions and microstructural growth behavior (e.g. dislocations, twin domains etc.) of ScN samples and when fabricated with other metals and/or TMNs as in metal/semiconductor superlattices, multilayers etc [1, 4, 18, 19].

* Corresponding author: mgupta@csr.res.in

In terms of defects, even though it is well known that

during the growth of ScN itself, finite incorporation of substitutional (O_N) and/or interstitial oxygen (O_i) is inherent regardless of T_s [16, 18, 20], but combined study of first principles density functional theory (DFT) with site occupancy disorder technique reveals that the electronic band structure of ScN remains unaltered despite of a shift of the Fermi energy level to the bottom of the conduction band [4]. Nonetheless, only recently, the primary contribution of oxygen incorporation has also been attributed to the surface oxidation [13, 17]. Howbeit, nitrogen vacancies (V_N) are known to form a defect energy level at ≈ 1.26 eV above the valence band maxima at Γ point of the Brillouin zone [21]. In this context, it is to be mentioned here that significance of high T_s depositions in suppression of defects were found to be conflicting in literature [13, 17, 22, 23], yet have not been highlighted so far.

Furthermore, as regards to technological viability in electronics viz. CMOS integrated circuits, plastic substrates etc, high T_s synthesis is highly undesirable [24]. Moreover, the extent of diffusion across the metal-semiconductor superlattice and/or multilayer interfaces will be comparatively high at a high T_s regime [12], which could limit the device performances in practical applications. Additionally, interdiffusion across film-substrate interfaces are also pronounced at high T_s depositions [21, 25]. In view of this, contrary to high T_s depositions, we adopted a room temperature deposited reactive magnetron sputtering technique for the synthesis of ScN thin film samples, as ScN favors thermodynamical growth conditions even at 298 K ($\Delta H_f^0 = -3.29$ eV). Such temperature regime also paves the way for precise control over variation of relative N_2 partial pressures (R_{N_2}) to probe the structural phase evolution from hexagonal close packed (hcp) Sc to rocksalt-type face centered cubic (fcc) ScN, which is still ambiguous.

In order to probe the electronic structure of ScN, so far, usually x-ray photoelectron spectroscopy (XPS) or soft x-ray absorption spectroscopy (SXAS) at N K-edge (401.6 eV) and Sc L-edge (402.2 eV) were considered [21, 26–28]. But, since the two absorption edges appear very close to each other and moreover, both XPS and SXAS are known to be surface sensitive techniques [29], an alternative powerful technique such as x-ray absorption fine structure (XAFS) can provide better insight on the metrical parameters at atomic scale level. With this motif, for the first time, XAFS was implemented on the Sc-N system complementary to SXAS to probe the K-edge of Sc in ScN. In spite of recent surge in investigation of various physical properties, further realization of variation of N were systematically demonstrated in terms of structural, electronic, optical and mechanical responses of room temperature deposited ScN thin film samples which are still missing in literature.

II. EXPERIMENTAL

Metallic Sc and a series of ScN thin film samples were deposited on amorphous quartz and single crystal Si (100) substrates at various R_{N_2} [= $P_{N_2}/(P_{N_2} + P_{Ar})$, where P_{N_2} and P_{Ar} are nitrogen and argon partial pressures, respectively] flow = 1.6, 2.5, 5, 10, 25, 50 and 100% in closed intervals using a direct current magnetron sputtering (dcMS) at ambient temperature (≈ 300 K). For thin film deposition, a Sc (99.95% pure) 3-inch target was sputtered in the presence of 5N purity Ar and/or N_2 gas flows. Prior to the deposition, the substrates were cleaned in an ultrasonic bath of acetone followed by methanol wiping with dry air blown and were loaded into the chamber. Subsequently, the sample holder was baked for 1 hour at 573 K and then cool down to room temperature to achieve a base-pressure of about 1×10^{-7} Torr or lower. During deposition, the working pressure was $\approx 3 \times 10^{-3}$ Torr and the substrate holder rotation was kept fixed at 60 rpm to get better uniformity of the samples.

For thickness calibration of the samples, x-ray reflectivity (XRR) measurements were performed using Cu-K α x-rays on a Bruker D8 Discover system. Once the deposition rate was obtained from the fitting of the XRR data (not shown), typically 200 nm thick samples were prepared following the similar deposition procedure. The structural characterization of samples were carried out using x-ray diffraction (XRD) using a Bruker D8 Advance XRD system based on θ - 2θ Bragg-Brentano geometry with Cu-K α (1.54 Å) x-rays and detected using a fast 1D detector (Bruker LynxEye). To probe the local electronic structure, surface sensitive SXAS measurements were performed at N K-edge and Sc L_(III,II)-edges in total electron yield (TEY) mode at BL-01 beamline of Indus-2 synchrotron radiation source [37] at RRCAT, Indore, India. Complementary to SXAS, to get an elementary insight probing the deep core level in atomic scale regime, x-ray absorption fine structure (XAFS) measurements were performed in fluorescence mode at BL-09 beamline at RRCAT, Indore, India and also at P64 beamline of PETRA-III, DESY, Germany [38]. XAFS data taken at Sc K-edge from both beamlines were found to be similar and XANES data taken at BL-09 and EXAFS data taken at P64 has been included. The obtained data was processed in Athena software [39] with pre and post-edge normalization [40] and fitting of the Fourier Transform (FT) spectra were performed using a software code developed by Conradson et al [41]. The fitted R range was taken from 0 to 10 Å, while the used k -range was 3 to 8 Å⁻¹.

The optical absorption spectra of the ScN thin film samples were recorded by Perkin Elmer, Lambda-750 UV-Visible spectrophotometer with double beam monochromator in the wavelength range of 250 - 1000 nm at room temperature. The reflectance of the recorded data were converted to absorption spectra using Kubelka-Munk radiative transfer model, which is associated with

TABLE I. Growth techniques of ScN thin film samples deposited using various substrate temperature (T_s) and deposition power (P) on different substrates with corresponding lattice parameter (LP) and direct optical bandgap (E_g) values. Here, dcMS = Direct current magnetron sputtering and MBE = Molecular beam epitaxy, RMS = Reactive magnetron sputtering, 300^\dagger = amorphous at 300 K, GGA-PBE = Perdew-Burke-Ernzerhof GGA exchange correlation functional, HSE06 = Heyd-Scuseria-Ernzerhof Hybrid functional, FLAWP = Full-potential linearized augmented plane wave method, FLAWP-GGA = Full-potential linearized augmented plane wave method with generalized gradient approximation, LDA = Local density approximation, GGA+U = Generalized gradient approximation with Hubbard U correction.

Exp. Tech.	Substrate	Process Parameters	LP (\AA)	E_g (eV)	Ref.
dcMS	MgO (001) & Si (001)	$T_s = 1103$ K, P = 150 W	4.50	-	[4]
dcMS	c-plane Al_2O_3 , MgO (111) & r-plane Al_2O_3	$T_s = 973 - 1223$ K, P = 125 W	4.504 - 4.512	-	[16]
dcMS	MgO (001)	$T_s = 1123$ & 1223 K, P = 60 - 300 W	4.50	2.18 - 2.7	[30]
dcMS	MgO (001)	$T_s = 973$ K	4.573	2.59	[26]
MBE	GaN (0001), SiC (0001) & AlN (0001)	$T_s = 1023$ K, P = 200 W	4.497	2.1	[15]
RMS	MgO (001)	$T_s = 823$ K, P = 25 - 127 W	4.52 - 4.54	2.1	[25]
dcMS	MgO (001)	$T_s = 873 - 1073$ K, P = 125 W	4.50	2.19 - 2.23	[17]
dcMS	c-plane Al_2O_3 & Si	$T_s = 300^\dagger - 1023$ K, P = 40 W	$\approx 4.47 - 4.52$	2.2 - 3.1	[17]
MBE	MgO (001),	$T_s = 1073$ K,	-	2.15	[31]
dcMS	Quartz & Si (100)	$T_s = 300$ K, P = 100 W	4.49 - 4.567	2.25 - 2.62	this work
Theoretical					
GGA-PBE & HSE06	-	-	4.519	2.02	[30]
FLAPW &	-	-	4.499	-	
FLAPW-GGA	-	-	4.42	-	[32]
LDA	-	-	4.50	-	
GGA+U	-	-	4.47	-	[33]
			4.52	1.86	[34]

the absorption coefficient (α) [42] of the ScN thin film samples. To measure the hardness and elastic modulus of the samples, nanoindentation tests (Anton Paar, Switzerland) were performed using Berkovich diamond indenter tip with standard loading and unloading procedure based on Oliver and Pharr model [43]. In order to suppress the substrate effects, the measurements were performed on one/tenth of the total sample thickness [44].

III. RESULTS

A. X-Ray Diffraction

To take into account the phase formation of as-deposited samples, Figure 1(a) illustrates the XRD data of Sc and ScN thin film samples and are compared with bulk references [30, 45], whereas, Figure 1(b) demonstrates the obtained variations in the lattice parameters (LP) and crystallite size as a function of R_{N_2} . In addition, the highlighted region (in cyan) of Figure 1(b) depicts the experimentally obtained LP of ScN thin film

samples in literature and the red dotted line is a guide to eye for the theoretical predicted value of bulk ScN [30]. As can be seen from Figure 1(a), the occurrence of three prominent peaks for Sc thin film sample can be assigned to (100), (002) and (101) reflection planes of hcp Sc, whereas for ScN samples, three different growth stages can be witnessed with variation in R_{N_2} flow namely, (i) interstitial incorporation of N atoms within hcp Sc, (ii) formation of NaCl rocksalt type fcc-ScN, and (iii) gradual expansion of ScN lattice due to incorporation of N atoms in fcc-ScN.

Here, it is to be mentioned that an earlier report on deposition of polycrystalline ScN thin film samples on quartz substrates at $T_s = 300$ K using rf magnetron sputtering have reported amorphous growth and later on tuning of T_s to high temperature resulted in preferential grain growth either along (111) or (200) plane, albeit the XRD data for the as-deposited samples were not presented therein [46]. However, in the present work, at a very initial stage of $R_{N_2} = 1.6\%$, the N atoms occupy the interstitial sites of hcp Sc manifesting an asymmetry and broadening in the reflection peak which suggests phase

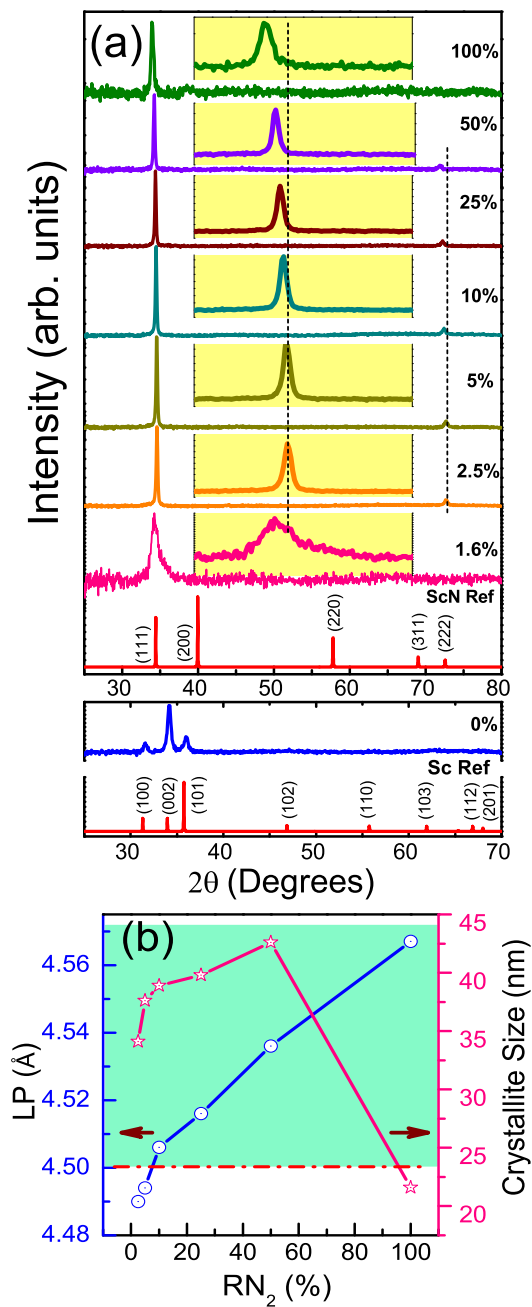


FIG. 1. XRD pattern(a) and obtained variations in the lattice parameters and crystallite size (b) as a function of R_{N_2} of pure Sc and ScN samples deposited at various $R_{N_2} = 1.6, 2.5, 5, 10, 25, 50$ and 100% .

co-existence of hcp Sc and fcc ScN at certain phase fractions (as could also be evidenced from our XAFS data) and an enhancement in the crystalline disorder. Later on, when R_{N_2} was increased to 2.5% , the sample exhibited a highly textured orientation with (111) and (222) reflection planes, resembling a rocksalt NaCl type structure even though the LP was 4.49 \AA , slightly less than the theoretically predicted value of 4.501 \AA [30]. With

further increase in R_{N_2} flow (from 5 to 50%), the texturing of the samples remain unaltered, but due to gradual incorporation of N atoms within the crystal lattice, it starts to expand as shown in Figure 1(a) by the gradual peak shifts of both (111) (magnified view shown in the highlighted inset) and (222) reflection peaks towards the lower diffraction angle (shown by dotted lines) accompanied with an increase in the crystallite size (Figure 1(b)).

Such unidirectional grain growth can be attributed to the kinetics driven mechanism at ambient temperature deposition ($\approx 300 \text{ K}$), due to trapping of the less mobile adatoms in the highest surface energy site i.e along the (111) reflection plane of ScN [47]. Besides, further increase in R_{N_2} at 100% flow causes lattice expansion in expense of reduced peak intensity of (111) reflection plane due to possible oversaturation of N, resulting in broadening of the (111) peak (as can be seen in highlighted region of Figure 1(a)) with reduced crystallite size (Figure 1(b)), and further absence of (222) grain growth suggests shattering of the long range periodicity. In view of growth evolution of Sc \rightarrow ScN at various R_{N_2} flow with electronic properties, SXAS measurements were performed and are discussed in section III B.

B. Soft X-Ray Absorption Spectroscopy

To get an insight on the local electronic structure of Sc and ScN thin film samples with variation in R_{N_2} flow, SXAS spectra of Sc L-edge and N K-edge were recorded and are shown in Figure 2(a), whereas, the first order derivative of the absorption spectra with respect to the photon energy is described in Figure 2(b). Additionally, to probe the oxidation effect, Figure 2(c) demonstrates the O K-edge XANES spectra of the samples. Here, it is to be mentioned that for a pure Sc sample, two absorption edges namely L_{III} and L_{II} are expected due to spin-orbit splitting of the Sc 2p orbital into $2p_{3/2}$ and $2p_{1/2}$ states in the absence of any ligand (C, N, O etc.) around the vicinity of Sc, a consequence of the transition of core electron from Sc $2p_{3/2} \rightarrow Sc 3d$ (L_{III}) and Sc $2p_{1/2} \rightarrow Sc 3d$ (L_{II}) states [48]. However, in the present case, the prominent features of Sc sample in Figure 2(a) and 2(b) marked as '1', '2', '3' and '4' can be assigned to L_{III} (t_{2g}), L_{III} (e_g), L_{II} (t_{2g}) and L_{II} (e_g) edges respectively due to the presence of a finite amount of unintentional O ligand field, which led to hybridization of Sc $3d$ -O $2p$ orbitals resulting in further splitting of each L_{III} and L_{II} features into t_{2g} and e_g .

Subsequently, the effect of surface oxidation/oxidation during the deposition itself for Sc sample is even pronounced from the O K-edge, where the doublet appearing at around 532.4 and 534.4 eV (shown by the pink highlight) can be inferred to t_{2g} (O $2p\pi + Sc3d$) and e_g (O $2p\sigma + Sc3d$) states due to the possible octahedral ligand field splitting ($10Dq$), whereas the broad feature 'D' arises due to hybridization of the O $2p$ with $4sp$ states of Sc [48, 49]. Similarly, for $R_{N_2} = 1.6\%$ sample, both

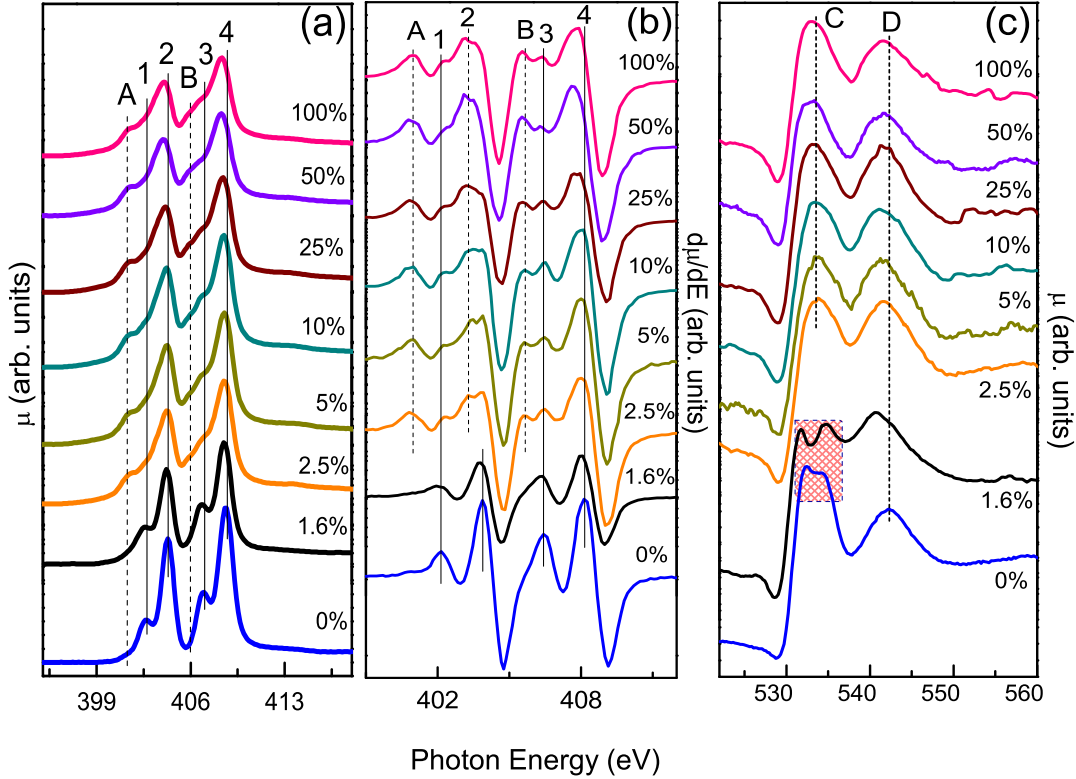


FIG. 2. Normalized SXAS spectra of Sc L_{III}, L_{II} and N K-edge (a), first order derivative of absorption spectra with respect to the photon energy (b) and O K-edge (c) of pure Sc and ScN samples deposited at various $R_{N_2} = 1.6, 2.5, 5, 10, 25, 50$ and 100%.

Sc L-edge and O K-edge features mimic the same trend as metallic Sc thin film sample, but an increase in $10Dq \approx 2.9(\pm 0.3)$ eV can be observed, which might be due to the shrink in volume of interstitial ScN during the process of structural transformation from Sc \rightarrow ScN. Hence, O K-edge spectra confirms the incorporation of bonded O on the sample surface which can be present either in the form of Sc_xO_y (for Sc)/ ScO_xN_y (for 1.6% ScN), but, certainly not Sc_2O_3 ($10Dq_{[Sc-O]} = 3.3$ eV), as both samples were of metallic grey in color (as opposed to transparent Sc_2O_3).

With further increase in R_{N_2} from 2.5 - 100%, as can be seen from Figure 2(a) and 2(b), two new pronounced features labelled as ‘A’ and ‘B’ arises which can be ascribed to ligand field splitting in the presence of N octahedral environment and noticeable reduction in the intensity of features ‘1’ and ‘3’ can be detected which can be better discerned from the O K-edge spectra. Here, instead of a doublet, a new feature ‘C’ can be noted. The appearance of similar experimental spectra have also been reported by Kumar et al. in the O K-edge of TiN ($T_s = 1023$ K) and through a combined study of DFT and ab-initio full potential multiscattering (FMS) theory, they concluded that such feature arises due to the presence of substitutional (O_N) and interstitial (O_i) oxygen in a

defect complex state ($4O_N + O_i$) [20]. Hence, the contribution of defects in early TMNs are comparable for both ambient and high T_s depositions. As mentioned earlier, since the N K-edge and Sc L-edge appears very close to each other, Nayak et al. have performed theoretical simulations based on the FMS theory and reported a value of $10Dq = 2.1$ eV [27], which is in well agreement with the experimentally observed value of $\approx 2.3(\pm 0.3)$ eV obtained in the present work. Even though, it appears from Figure 2(a) that the energy features of ‘2’ and ‘4’ remain almost unaltered with an increase in R_{N_2} flow (2.5% and above), but first order derivatives of the absorption spectra divulged a diverse profile where a new feature (around ‘2’ and less pronounced for feature ‘4’) towards the lower energy side for these samples is clearly visible as evidenced from Figure 2(b), which can be attributed as L_{III} (e_g) and L_{II} (e_g) corresponding to Sc-N bonds. Considering the new features of ScN, the spin-orbit splitting comes out to be $4.8(\pm 0.3)$ eV, well in agreement as reported for ScN [28].

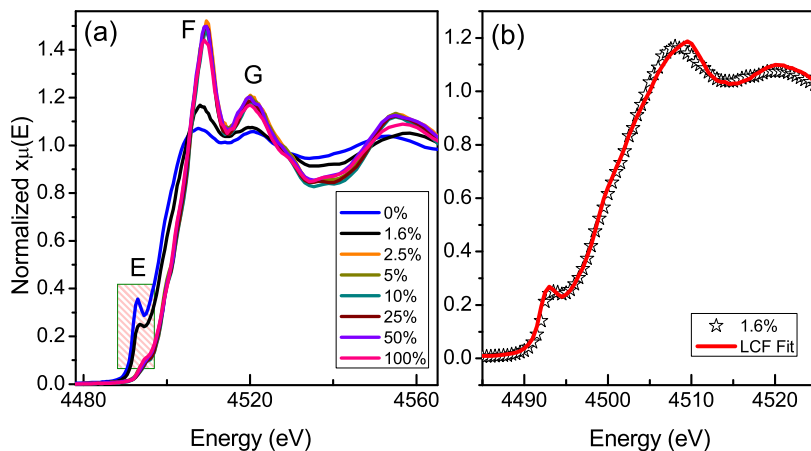


FIG. 3. Normalized Sc K-edge XAFS spectra of metallic Sc and ScN thin film samples deposited at various $R_{N_2} = 1.6, 2.5, 5, 10, 25, 50$ and 100% (a) and linear combination fit (LCF) of 1.6% sample.

C. X-Ray Absorption Fine Structure

So as to achieve complementary information about the electronic structure, Figure 3(a) depicts the normalized Sc K-edge XANES spectra of Sc and ScN samples deposited at various R_{N_2} flow and Figure 3(b) shows the linear combination fit (LCF) of 1.6% sample. The spectra of Sc and 1.6% ScN sample shows distinct features in comparison to samples deposited at relatively high R_{N_2} flow. In the pre-edge region, an intense feature ‘E’ can be seen for Sc sample and with R_{N_2} flow at 1.6%, it gets feeble. Such intense pre-edge feature has previously been reported for metallic hcp Ti (for both foil and film) with hexagonal symmetry and has been attributed to $1s \rightarrow 3d$ electric quadrupole transition ($\Delta l = \pm 2$) [50, 51]. It is conventional that pre-edge features differ due to different geometrical parameters such as, inversion symmetry, co-ordinations and bonding configurations (e.g. bond length, bond angles) etc [52]. For 1.6% sample, the best fit was obtained considering the phase co-existence of both Sc (71.9(± 0.9))% and ScN (28.1(± 0.9))% phases.

On the contrary, with further incorporation of N, the intensity gradually reduces from $R_{N_2} = 1.6\%$ to 2.5%, and are alike for rest of the samples. Since, it is well established that Sc is bonded with nearest neighbor N atoms in an octahedral co-ordination sphere with inversion symmetry [28], the emergence of weak pre-edge feature can be ascribed to $1s$ core electron transition to $3d$ states of the absorber having a partial contribution from the $2p$ orbitals of N under the allowed electric dipole transition scheme ($\Delta l = \pm 1$), like in TiN [53].

In addition, nitridation of the samples consequences in continuous shift of the absorption edge ($E_0 =$ taken at 50% of the absorption spectra) [54] towards the higher energy side at $E_0 = 4496(\pm 0.3)$ (Sc), $4497.4(\pm 0.3)$ ($R_{N_2} = 1.6\%$) and $4500.3(\pm 0.3)$ ($R_{N_2} = 2.5\%$) eV which can be interpreted in terms of higher core-hole screening due to increase in valence states of Sc from Sc \rightarrow ScN. How-

ever, above the absorption edge in the XANES region, the feature ‘F’ and ‘G’ can be assigned to $1s \rightarrow 4p$ electric dipole allowed transitions of a core electron as evidenced for other transition metal compounds e.g. TiC [55]. A diverse trend of feature ‘F’ can be attributed to the different stacking sequence of Sc (ABAB for hcp) and ScN (ABCABC for fcc) samples, where higher fcc phase fractions result in sharp intense peak (characteristic features of TMNs) in comparison to diffuse kind of feature for Sc thin film samples [56, 57], due to a possible intermixing between $3d$ quadrupole and $4p$ dipole states [29]. It is worth mentioning here that in the present study, Sc K-edge of pure Sc thin film sample does not replicate the XAFS spectra of Sc_2O_3 studied by Chassé et al [58], consistent with our XRD data analysis. Since, fluorescence detected XAFS is known to be a bulk sensitive technique with penetration depth ranging in micrometers [51] compared to surface sensitive SXAS where the depth scale ranges only in nanometer scale (≈ 10 nm) [29], the averaged out bulk information from the XAFS data further confirms the presence of higher surface oxidation in the samples as was evidenced from the Sc L-edge and O K-edge SXAS spectra.

Figure 4(a) and (b) shows the Fourier Transform (FT) moduli $|\chi(R)|$ and the real component $[\text{Re } \chi(R)]$ of the Sc K-edge EXAFS spectra as a function of radial distance ($R-\phi$) and the corresponding best fit, whereas, Figure 4(c) demonstrates the $\chi(k) \times k^3$ spectra. For fitting, hcp and cubic rocksalt type NaCl structure of Sc and ScN were considered having space groups of $P63/mmc$ [59] and $Fm\bar{3}m$ [15], respectively. The fitting was performed using LP obtained from the XRD data and the obtained metrical parameters are tabulated in Table II.

For Sc sample, the single shell of FT spectra corresponds to Sc co-ordinated to $7.2(\pm 1.8)$ Sc atoms each having an atomic pair distance of $3.25(\pm 0.02)$ Å. Hence, the local co-ordination environment is rather in a distorted hexagonal symmetry which might be responsible

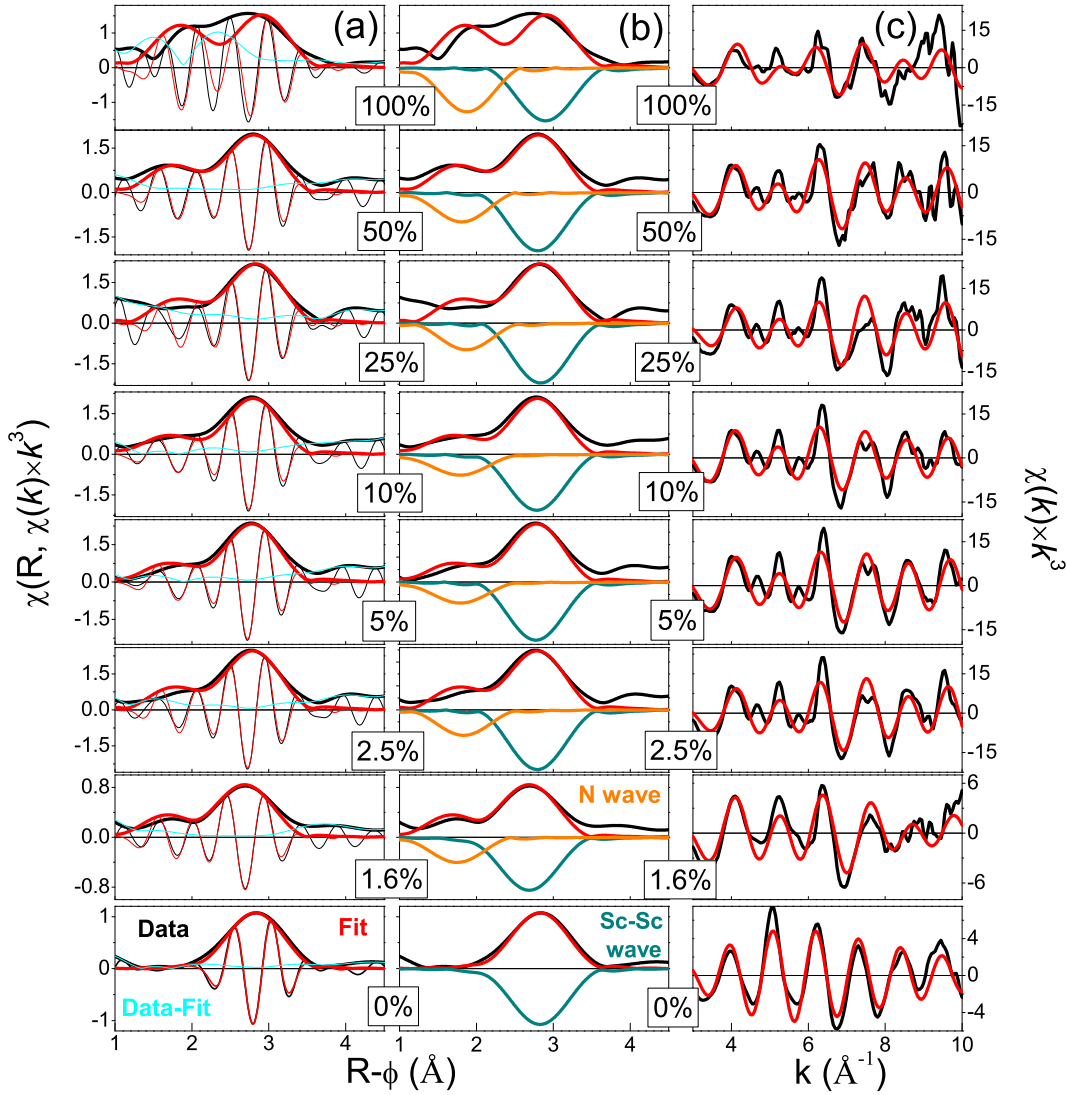


FIG. 4. Comparison of Fourier transform (FT) moduli $\chi(R)$ (a), $\text{Re}[\chi(R)]$ (b) in the R range and $\chi(k) \times k^3$ spectra in the k range (c) of Sc and ScN thin film samples deposited at various $R_{N_2} = 2.5, 5, 10, 25, 50$ and 100% .

for an intense pre-edge feature across the Sc K-edge absorption spectra (Figure 3). In addition, for ScN, considering a theoretical LP of $a^* = 4.501 \text{ \AA}$ [15, 30], the first and second nearest neighbor distances can be anticipated at $R_{\text{Sc-N}}^* = a/2 = 2.25 \text{ \AA}$ and $R_{\text{Sc-Sc}}^* = a/\sqrt{2} = 3.18 \text{ \AA}$ [60]. As can be seen from Figure 4(a) and (b), the two consecutive maxima distributed over $R-\phi = 1 - 3.9 \text{ \AA}$ range correspond to the first Sc-N and second Sc-Sc nearest neighbor bonds. For 1.6% sample, even though it was not possible to obtain the structural parameters from the XRD data due to appearance of a single broad peak, but the obtained EXAFS fitting parameters from Table II clearly states the interstitial nature of the sample with less content of both N and Sc atoms in the first and second shell co-ordinations to fully evolve to the fcc phase considering only the ScN phase during fitting. Apparently, at higher R_{N_2} flow (above 2.5%), all ScN samples

typically exhibit the octahedral inversion symmetry as expected in NaCl structure and corroborates well with our XRD data within the experimental resolution, as expected. To take into account the optical and mechanical response of the ScN samples, UV-Vis measurements along with nanoindentation tests were performed and are discussed in section III D.

D. Optical & Mechanical Behavior

In order to delve the optical properties with electronic structure, Figure 5(a) shows the Tauc's plot curve of α as a function of incident photon energy for ScN thin film samples deposited at $R_{N_2} = 2.5, 5, 10, 25, 50$ and 100% flows. The optical bandgap values were obtained from the intersection of the energy axis by extrapolating the lin-

TABLE II. The metrical parameters obtained from the fitting of the EXAFS data recorded at Sc K-edge. Considering the central atom as Sc, here, N and N' = first and second nearest neighbor co-ordination, R_{Sc-N} and R_{Sc-Sc} = atomic pair distance of the first and second neighbors i.e. Sc-N and Sc-Sc, σ_{Sc-N} and σ_{Sc-Sc} = root mean square displacement obtained from fitting of the first and second shell.

R_{N_2} (%)	N	R_{Sc-N} (Å)	σ_{Sc-N} (Å)	N'	R_{Sc-Sc} (Å)	σ_{Sc-Sc} (Å)
0%	-	-	-	7.23	3.25	0.098
	-	-	-	(±1.82)	(±0.02)	(±0.01)
1.6%	2.252	2.189	0.064	5.78	3.136	0.098
	(±0.676)	(±0.025)	(±0.031)	(±1.59)	(±0.021)	(±0.017)
2.5%	4.48	2.25	3.358	9.25	3.20	0.06
	(±1.34)	(±0.02)	-	(±2.55)	(±0.02)	(±0.02)
5%	7.42	2.23	2.488	8.93	3.19	0.06
	(±2.22)	(±0.03)	(±0.03)	(±2.42)	(±0.02)	(±0.02)
10%	8.03	2.23	0.11	9.40	3.20	0.07
	(±2.4)	(±0.03)	(±0.03)	(±2.6)	(±0.02)	(±0.02)
25%	5.12	2.27	0.06	7.46	3.23	0.04
	(±1.5)	(±0.03)	(±0.03)	(±2.14)	(±0.02)	(±0.02)
50%	5.86	2.23	0.07	8.25	3.21	0.07
	(±1.75)	(±0.03)	-	(±2.3)	(±0.02)	(±0.02)
100%	7.61	2.28	0.07	5.39	3.27	0.05
	(±2.28)	(±0.02)	-	(±1.62)	(±0.02)	(±0.03)

ear least square fitting curve around the inflection point using the Tauc relation, $\alpha h\nu = A (h\nu - E_g)^{\frac{1}{2}}$ for direct transitions [61] where, $h\nu$ = photon energy, E_g = optical bandgap and A is proportionality constant. As mentioned earlier in section III B, both Sc and 1.6% ScN sample were metallic in nature and did not show any absorption in the whole energy spectrum. Beyond $R_{N_2} = 1.6\%$, all the samples showed semiconducting behavior with a well-defined optical bandgap. In this context, it is to be mentioned that ScN exhibits an indirect bandgap of 0.9 eV [31, 62], whereas, two direct bandgaps at 2.2 and 3.8 eV were reported [3, 30]. Generally, only the first direct bandgap has been reported (see Table I) and will also be considered in this work. The large variation in the reported bandgap values have been attributed either to the formation of defect states near the conduction band for n-type degenerate semiconductor termed as 'Burstein-Moss band filling effect' [63] or to the strain mediated effects which can modulate the energy band shifts to a certain extent [64]. The trend was non-linear in nature with a maximum value of 2.62 eV for 5% ScN sample and a minimum of 2.25 eV for sample deposited at $R_{N_2} = 100\%$. Thus, the variations in the bandgap values in the present study can be inferred primarily to the contribution of defects as the stress-strain mediated changes might be negligible in the present case, as all the samples were deposited on amorphous quartz substrates. It is worth mentioning here that the bandgap values of ScO_xN_y and Sc_2O_3 are reported to be 3.25 eV and 5.6 eV, respectively [27], which are way higher than the obtained bandgaps in the present study.

Figure 5(b) demonstrates the measured indentation hardness (H) and modulus (E) of the ScN thin film samples as a function of R_{N_2} whereas, Figure 5(c) illustrates the ratio of (H^3/E^2) which corresponds to the resistance

of ScN samples to plastic deformation as a function of H. As expected, Sc exhibits the lowest H and E values of $8(\pm 1.3)$ and $79(\pm 7)$ GPa, respectively. With nitridation, both H and E increases monotonically from 15 - 27 GPa and 152 - 268 GPa for the ScN samples, except for $R_{N_2} = 2.5\%$, which is close to the calculated value of 25 GPa for ScN [65]. At $R_{N_2} = 2.5\%$, the values maximizes at $34(\pm 6.2)$ and $476(\pm 157)$ GPa, respectively, which can be attributed to the highest density as estimated from the XRD data [66], smaller grain size and strong (111) and (222) texturing of the ScN sample [67]. With increase in $R_{N_2} = 2.5 - 50\%$, from the XRD data (Figure 1), it is evident that the XRD peaks shift chronically along the lower diffraction angle demonstrating in-plane compressive residual stress. In addition, the texturing effect is well retained, which is known to be the highest density plane and the corresponding H is considered to be the highest along the (111) plane [68] and are the reasons behind the increase in H. Even though, the texturing effect is witnessed for $R_{N_2} = 100\%$ sample only along the (111) plane, but the decrease in grain size in turn elevates the grain boundaries which could lead to plausible rise in H value [67]. Furthermore, the gradual rise in E values from Sc→ScN can be attributed to the strong covalent bond formation of Sc-N than metallic Sc-Sc bonds in Sc [44], as evidenced from our XAFS study. Apart from this, the ScN thin film samples also show a propitious resistance to plastic deformation (H^3/E^2) following a linear trend with increase in H values [69]. However, it is to be mentioned here that typically the values of H and E are likely comparable in the range of $R_{N_2} = 2.5 - 100\%$ within the error bars.

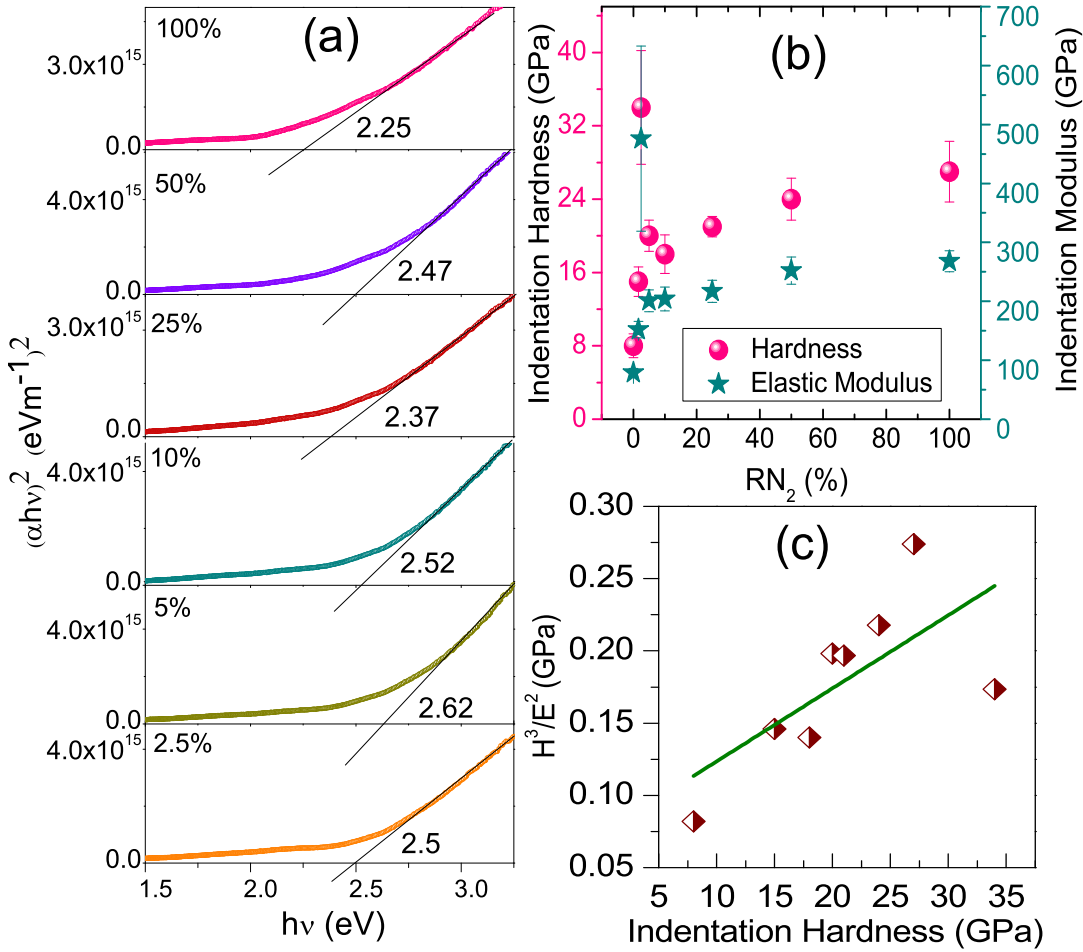


FIG. 5. Obtained direct bandgaps from the Tauc's plot of the absorption co-efficient as a function of incident photon energy (a), nano-indentation hardness and modulus with error bars (b) and the ratio of (H^3/E^2) depicting resistance to plastic deformation of ScN thin film samples as a function of hardness (c), deposited at room-temperature at various $R_{N_2} = 1.6, 2.5, 5, 10, 25, 50$ and 100% flow.

IV. DISCUSSION

At an early stage of subtle nitridation ($R_{N_2} = 1.6\%$), combined XRD and XAFS study reveal formation of an interstitial compound in the intermediate stage during evolution from hcp Sc to fcc ScN and with higher content of N, at $R_{N_2} = 2.5\%$ and above, adaptation of fcc phase with octahedral symmetry were observed. Here, it is interesting to note that likewise in early TMNs, ScN does not possess bimetallic phases (e.g. Ti_2N , V_2N and Cr_2N) at ambient temperature and pressure, and rather manifests a large homogeneity range (retaining NaCl type rocksalt crystal structure from as low as $R_{N_2} = 2.5\%$ to as high as 100%). In contrary, with increase in N_2 atomic %, the overall crystal lattice withstands a minimal lattice expansion of only $\approx 1.7\%$ at highest $R_{N_2} = 100\%$ for ScN. It could be well discerned in terms of higher interstitial lattice volume of ScN compared to other early TMNs in the series (TiN, VN and CrN). Since, the early

TMNs exhibit NaCl type rocksalt crystal structure, the corresponding octahedral interstitial site occupancy of nitrogen atoms would be at edge centers of the unit cell i.e. at $(\frac{1}{2}, 0, 0)$, $(0, \frac{1}{2}, 0)$, $(0, 0, \frac{1}{2})$ and at the center i.e. $(\frac{1}{2}, \frac{1}{2}, \frac{1}{2})$ position of the respective unit cell. Considering the (100) lattice plane of the unit cell, from the simple pictorial overview as shown in Figure 6 for ScN sample, the radius of the interstitial site (R_{int}) can be similarly evaluated for early TMNs by solving two basic equations along the edge and diagonal as,

$$R_{TM} + 2R_{int} + R_{TM} = a, \dots(i)$$

and,

$$R_{TM} + 2R_{TM} + R_{TM} = (a^2 + a^2)^{\frac{1}{2}}, \dots(ii)$$

where, R_{TM} = radius of TM atom, and a = LP of TMN. Hence, the corresponding structural parameters of the early TMNs are enlisted in Table III.

TABLE III. Early transition metals (TM) and their corresponding crystal structures (CS) and lattice parameters (LP_{TM}). In comparison to metal counterparts, lattice parameters (LP_{TMN}) of their nitrides with calculated radius of interstitial octahedral site (R_{int}) have been tabulated below.

TM	CS	LP_{TM} (Å)	TMN	LP_{TMN} (Å)	R_{int} (Å)	Ref.
Sc	hcp	$a = b = 3.309,$ $c = 5.273$	ScN	4.501	0.659	[70]
Ti	hcp	$a = b = 2.951,$ $c = 4.684$	TiN	4.24	0.621	[71]
V	bcc	$a = 3.03$	VN	4.139	0.606	[66]
Cr	bcc	$a = 2.885$	CrN	4.14	0.606	[72]

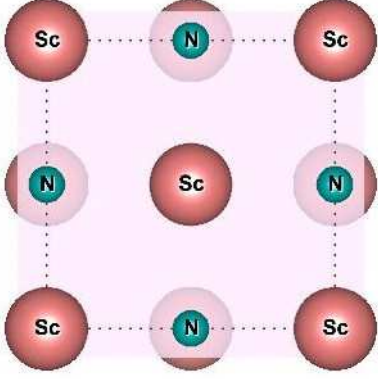


FIG. 6. Representative unit cell of ScN (100) crystal plane

From Table III, it is evident that ScN exhibits the largest unit cell with higher fraction of interstitial volume among the early TMNs, leading to a large homogeneity range for retaining the fcc rocksalt phase accompanied with minuscule lattice expansion. In this context, it is worth mentioning that Al et al. have reported that ScN can withstand upto $\approx 20\%$ of N vacancies within the crystal lattice [73]. Such a large homogeneity range has also been witnessed for other early TMNs like TiN_x ($0.67 \leq x \leq 1.3$) [74], VN_x ($0.79 \leq x \leq 0.96$) [75] etc. in the octahedral symmetry. In addition, combined SXAS study at Sc L-edge, N K-edge and O K-edge reveal that the effect of oxidation is less pronounced for nitrided samples compared to their metal/interstitial counterparts. This is due to formation of strong Sc-N covalent bonds which results in relatively high Gibb's energy for oxide formation (-6.48 eV) of ScN than metallic Sc-Sc bonds in pure Sc (-9.43 eV) at ≈ 298 K [13]. Furthermore, our Sc K-edge XANES spectra confirms distinct evolution from hexagonal to octahedral symmetry complemented with a clear rise in the valence state for ScN samples consistent with our XRD results. The pre-edge features of neither Sc nor ScN resembles the Sc K-edge oxide spectra [58] emphasizing on the higher surface oxidation effect in all these samples. Nonetheless, the local electronic structure as recorded from EXAFS replicates the XRD data with further insight on the presence of local defects in the vicinity of Sc atoms but the visible changes are however

marginal for all the samples. Even so, the non-monotonic variations in the optical bandgaps across the whole R_{N_2} range have no clear trend and in this scenario, it is difficult to correlate them in terms of defects as in case of polycrystalline thin film samples, the role of defects are always expected to be higher than epitaxial ScN thin film samples studied so far. Howbeit, the bandgap values in the present study lie well within the energy regime of ScN thin film samples as observed for high T_s depositions on single crystal substrates. Additionally, the hardness and indentation modulus agrees well during the evolution from Sc \rightarrow ScN with a linearly increasing trend of resistance to plastic deformation and also matches well with those reported in the literature [76, 77] within the experimental error bars.

CONCLUSION

In lieu of adoption of high temperature depositions hitherto, as-deposited ScN thin film samples exhibited highly textured orientation along the (111) and (222) reflection planes grown on amorphous quartz substrates due to preferable highest surface energy configuration at low temperature regime (here 300 K). SXAS study reveals pronounced incorporation of oxygen in metallic Sc and interstitial ScN sample deposited at $R_{N_2} = 1.6\%$ flow, although reduction of oxygen content can be witnessed with nitridation of the samples ($R_{N_2} = 2.5 - 100\%$). Complementary XAFS study shows distinct evolution from Sc \rightarrow ScN, where an intense pre-edge feature stems from non-centrosymmetric distortion for Sc and interstitial ScN ($R_{N_2} = 1.6\%$) sample, whereas, octahedral symmetry was retained by rest of the ScN samples deposited at higher R_{N_2} flow. From UV-Vis measurement, the obtained direct optical bandgaps were found to vary between 2.25 - 2.62 eV for $R_{N_2} = 2.5 - 100\%$, well in agreement with the values routinely reported in literatures for epitaxial ScN thin film samples. Even so, the nano-indentation measurements validates the high hardness of highly elastic ScN thin film samples ranging between 15 - 34 GPa with a monotonically increasing trend in the value of resistance to plastic deformations. In turn, the large homogeneity range of Sc-N system has been compared with elemental early 3d transition metal

nitride series viz. TiN, VN and CrN to comprehend the phase stability of cubic NaCl rocksalt type structure of ScN thin film samples over large variation in R_{N_2} flow. Hence, cumulative inferences drawn from this work can be epitomized as high vacuum deposition is imperative for high quality ScN samples but an alternate room temperature deposition can be adopted as opposed high T_s , to minimize the unintentional diffusion mechanisms at elevated temperatures finding applications in electronics viz. CMOS integrated circuits, free standing films on plastic substrates.

ACKNOWLEDGMENTS

Authors (SC and RG) are grateful to UGC-DAE CSR, Indore for providing financial support through CSR-IC-BL-62/CSR179-2016-17/843 project. Thanks are due to V. R. Reddy and Anil Gome for XRR measurements, Rakesh Sah for SXAS measurement at BL-01, Indus 2, RRCAT and Layanta Behera for various experiments. SC is thankful to Sanjay Nayak for fruitful discussions and Yogesh Kumar for his extended help in XRD and XAFS measurements. We also thank S. Tokekar, A. J. Pal, A. K. Sinha, D. M. Phase, V. Ganesan and V. Sathe for their kind support and constant encouragements.

-
- [1] B. Saha, A. Shakouri, T. D. Sands, Rocksalt nitride metal/semiconductor superlattices: A new class of artificially structured materials, *Applied Physics Reviews* 5 (2018) 021101.
- [2] P. Patsalas, N. Kalfagiannis, S. Kassavetis, G. Abadias, D. Bellas, C. Lekka, E. Lidorikis, Conductive nitrides: Growth principles, optical and electronic properties, and their perspectives in photonics and plasmonics, *Materials Science and Engineering: R: Reports* 123 (2018) 1–55.
- [3] B. Biswas, B. Saha, Development of semiconducting ScN, *Physical Review Materials* 3 (2019) 020301.
- [4] P. V. Burmistrova, J. Maassen, T. Favaloro, B. Saha, S. Salamat, Y. Rui Koh, M. S. Lundstrom, A. Shakouri, T. D. Sands, Thermoelectric properties of epitaxial ScN films deposited by reactive magnetron sputtering onto MgO (001) substrates, *Journal of Applied Physics* 113 (2013) 153704.
- [5] F. Scholz, Semipolar GaN grown on foreign substrates: a review, *Semiconductor Science and technology* 27 (2012) 024002.
- [6] M. Little, M. Kordesch, Band-gap engineering in sputter-deposited $Sc_xGa_{1-x}N$, *Applied Physics Letters* 78 (2001) 2891–2892.
- [7] J. Su, F. Niekiet, S. Fichtner, L. Thormaehlen, C. Kirchof, D. Meyners, E. Quandt, B. Wagner, F. Lofink, AlScN-based MEMS magnetoelectric sensor, *Applied Physics Letters* 117 (2020) 132903.
- [8] F. Tasnádi, B. Alling, C. Höglund, G. Wingqvist, J. Birch, L. Hultman, I. A. Abrikosov, Origin of the anomalous piezoelectric response in wurtzite $Sc_xAl_{1-x}N$ alloys, *Physical review letters* 104 (2010) 137601.
- [9] V. Rawat, Y. K. Koh, D. G. Cahill, T. D. Sands, Thermal conductivity of (Zr, W) N/ScN metal/semiconductor multilayers and superlattices, *Journal of Applied Physics* 105 (2009) 024909.
- [10] A. Belosludtsev, K. Juškevičius, L. Ceizaris, R. Samuilovas, S. Stanionytė, V. Jasulaitienė, S. Kičas, Correlation between stoichiometry and properties of scandium oxide films prepared by reactive magnetron sputtering, *Applied Surface Science* 427 (2018) 312–318.
- [11] B. Saha, M. Garbrecht, J. A. Perez-Taborda, M. H. Fawey, Y. R. Koh, A. Shakouri, M. Martin-Gonzalez, L. Hultman, T. D. Sands, Compensation of native donor doping in ScN: Carrier concentration control and p-type ScN, *Applied Physics Letters* 110 (2017) 252104.
- [12] P. Eklund, S. Kerdsonpanya, B. Alling, Transition-metal-nitride-based thin films as novel energy harvesting materials, *Journal of Materials Chemistry C* 4 (2016) 3905–3914.
- [13] J. More-Chevalier, S. Cichoň, L. Horák, J. Bulř, P. Hubík, Z. Gedeonová, L. Fekete, M. Poupon, J. Lančok, Correlation between crystallization and oxidation process of ScN films exposed to air, *Applied Surface Science* 515 (2020) 145968.
- [14] D. Rao, B. Biswas, E. Flores, A. Chatterjee, M. Garbrecht, Y. R. Koh, V. Bhatia, A. I. K. Pillai, P. E. Hopkins, M. Martin-Gonzalez, et al., High mobility and high thermoelectric power factor in epitaxial ScN thin films deposited with plasma-assisted molecular beam epitaxy, *Applied Physics Letters* 116 (2020) 152103.
- [15] J. Casamento, J. Wright, R. Chaudhuri, H. Xing, D. Jena, Molecular beam epitaxial growth of scandium nitride on hexagonal SiC, GaN, and AlN, *Applied Physics Letters* 115 (2019) 172101.
- [16] A. Le Febvrier, N. Tureson, N. Stalkerich, G. Greczynski, P. Eklund, Effect of impurities on morphology, growth mode, and thermoelectric properties of (1 1 1) and (0 0 1) epitaxial-like ScN films, *Journal of Physics D: Applied Physics* 52 (2018) 035302.
- [17] D. Rao, B. Biswas, S. Acharya, V. Bhatia, A. I. K. Pillai, M. Garbrecht, B. Saha, Effects of adatom mobility and Ehrlich–Schwoebel barrier on heteroepitaxial growth of scandium nitride (ScN) thin films, *Applied Physics Letters* 117 (2020) 212101.
- [18] Y. Kumagai, N. Tsunoda, F. Oba, Point defects and p-type doping in ScN from first principles, *Physical Review Applied* 9 (2018) 034019.
- [19] S. Acharya, A. Chatterjee, V. Bhatia, A. I. K. Pillai, M. Garbrecht, B. Saha, Twinned growth of ScN thin films on lattice-matched GaN substrates, *Materials Research Bulletin* (2021) 111443.
- [20] R. Kumar, S. Nayak, M. Garbrecht, V. Bhatia, A. Indiradevi Kamalasanan Pillai, M. Gupta, S. Shivaprasad, B. Saha, Clustering of oxygen point defects in transition metal nitrides, *Journal of Applied Physics* 129 (2021) 055305.
- [21] M. S. Haseman, B. A. Noesges, S. Shields, J. S. Cetnar, A. N. Reed, H. A. Al-Atabi, J. H. Edgar, L. J. Brillson, Cathodoluminescence and x-ray photoelectron spectroscopy of ScN: Dopant, defects, and band structure,

- APL Materials 8 (2020) 081103.
- [22] M. Moram, Z. Barber, C. Humphreys, The effect of oxygen incorporation in sputtered scandium nitride films, *Thin Solid Films* 516 (2008) 8569–8572.
- [23] T. Ohgaki, K. Watanabe, Y. Adachi, I. Sakaguchi, S. Hishita, N. Ohashi, H. Haneda, Electrical properties of scandium nitride epitaxial films grown on (100) magnesium oxide substrates by molecular beam epitaxy, *Journal of Applied Physics* 114 (2013) 093704.
- [24] S.-L. Tsai, T. Hoshii, H. Wakabayashi, K. Tsutsui, T.-K. Chung, E. Y. Chang, K. Kakushima, Room-temperature deposition of a poling-free ferroelectric AlScN film by reactive sputtering, *Applied Physics Letters* 118 (2021) 082902.
- [25] J. S. Cetnar, A. N. Reed, S. C. Badescu, S. Vangala, H. A. Smith, D. C. Look, Electronic transport in degenerate (100) scandium nitride thin films on magnesium oxide substrates, *Applied Physics Letters* 113 (2018) 192104.
- [26] J. More-Chevalier, S. Cichoń, J. Bulír, M. Poupon, P. Hubík, L. Fekete, J. Lančok, Electrical and optical properties of scandium nitride nanolayers on MgO (100) substrate, *AIP Advances* 9 (2019) 015317.
- [27] S. Nayak, M. Baral, M. Gupta, J. Singh, M. Garbrecht, T. Ganguli, S. Shivaprasad, B. Saha, Rigid-band electronic structure of scandium nitride across the n-type to p-type carrier transition regime, *Physical Review B* 99 (2019) 161117.
- [28] B. Biswas, S. Nayak, V. Bhatia, A. I. K. Pillai, M. Garbrecht, M. H. Modi, M. Gupta, B. Saha, Interfacial chemistry and electronic structure of epitaxial lattice-matched TiN/Al_{0.72}Sc_{0.28}N metal/semiconductor superlattices determined with soft x-ray scattering, *Journal of Vacuum Science & Technology A: Vacuum, Surfaces, and Films* 38 (2020) 053201.
- [29] G. S. Henderson, F. M. De Groot, B. J. Moulton, X-ray absorption near-edge structure (xanes) spectroscopy, *Reviews in Mineralogy and Geochemistry* 78 (2014) 75–138.
- [30] R. Deng, B. Ozsdolay, P. Zheng, S. Khare, D. Gall, Optical and transport measurement and first-principles determination of the ScN band gap, *Physical Review B* 91 (2015) 045104.
- [31] H. A. Al-Britthen, A. R. Smith, D. Gall, Surface and bulk electronic structure of ScN (001) investigated by scanning tunneling microscopy/spectroscopy and optical absorption spectroscopy, *Physical Review B* 70 (2004) 045303.
- [32] C. Stampfl, W. Mannstadt, R. Asahi, A. J. Freeman, Electronic structure and physical properties of early transition metal mononitrides: Density-functional theory LDA, GGA, and screened-exchange LDA FLAPW calculations, *Physical Review B* 63 (2001) 155106.
- [33] D. Gall, M. Stoehr, J. Greene, Vibrational modes in epitaxial Ti_{1-x}Sc_xN (001) layers: an ab initio calculation and Raman spectroscopy study, *Physical Review B* 64 (2001) 174302.
- [34] B. Saha, J. Acharya, T. D. Sands, U. V. Waghmare, Electronic structure, phonons, and thermal properties of ScN, ZrN, and HfN: A first-principles study, *Journal of Applied Physics* 107 (2010) 033715.
- [35] C. Braun, Parratt 32 Program for Reflectivity Fitting, Hahn-Meitner Institute, Berlin (1999).
- [36] L. G. Parratt, Surface studies of solids by total reflection of X-rays, *Physical Review B* 95 (1954) 359–369.
- [37] D. M. Phase, M. Gupta, S. Potdar, L. Behera, R. Sah, A. Gupta, Development of soft X-ray polarized light beamline on Indus-2 synchrotron radiation source, *AIP Conference Proceedings* 1591 (2014) 685–686.
- [38] W. A. Caliebe, V. Murzin, A. Kalinko, M. Görlitz, High-flux XAFS-beamline P64 at PETRA III, in: *AIP conference proceedings*, volume 2054, AIP Publishing LLC, 2019, p. 060031.
- [39] B. Ravel, M. Newville, ATHENA, ARTEMIS, HEP-HAESTUS: data analysis for X-ray absorption spectroscopy using IFEFFIT, *Journal of Synchrotron Radiation* 12 (2005) 537–541.
- [40] B. K. Teo, Extended x-ray absorption fine structure (EXAFS) spectroscopy: techniques and applications, in: *EXAFS Spectroscopy*, Springer, 1981, pp. 13–58.
- [41] S. D. Conradson, T. Durakiewicz, F. J. Espinosa-Faller, Y. Q. An, D. A. Andersson, A. R. Bishop, K. S. Boland, J. A. Bradley, D. D. Byler, D. L. Clark, et al., Possible Bose-condensate behavior in a quantum phase originating in a collective excitation in the chemically and optically doped Mott-Hubbard system UO_{2+x}, *Physical Review B* 88 (2013) 115135.
- [42] A. Murphy, Band-gap determination from diffuse reflectance measurements of semiconductor films, and application to photoelectrochemical water-splitting, *Solar Energy Materials and Solar Cells* 91 (2007) 1326–1337.
- [43] R. Ramaseshan, F. Jose, S. Rajagopalan, S. Dash, Preferentially oriented electron beam deposited TiN thin films using focused jet of nitrogen gas, *Surface Engineering* 32 (2016) 834–839.
- [44] P. Panda, R. Ramaseshan, Effects of Cr doping on the mechanical properties of AlN films grown by the co-sputtering technique, *Ceramics International* 45 (2019) 1755–1760.
- [45] F. H. Spedding, A. Daane, K. Herrmann, The crystal structures and lattice parameters of high-purity scandium, yttrium and the rare earth metals, *Acta Crystallographica* 9 (1956) 559–563.
- [46] X. Bai, M. Kordesch, Structure and optical properties of ScN thin films, *Applied surface science* 175 (2001) 499–504.
- [47] D. Gall, I. Petrov, L. Madsen, J.-E. Sundgren, J. Greene, Microstructure and electronic properties of the refractory semiconductor ScN grown on MgO (001) by ultra-high-vacuum reactive magnetron sputter deposition, *Journal of Vacuum Science & Technology A: Vacuum, Surfaces, and Films* 16 (1998) 2411–2417.
- [48] J. G. Chen, NEXAFS investigations of transition metal oxides, nitrides, carbides, sulfides and other interstitial compounds, *Surface Science Reports* 30 (1997) 1–152.
- [49] F. De Groot, J. Fuggle, B. Thole, G. Sawatzky, L_{2,3} x-ray-absorption edges of d₀ compounds: K⁺, Ca²⁺, Sc³⁺, and Ti⁴⁺ in O_h (octahedral) symmetry, *Physical Review B* 41 (1990) 928.
- [50] Z. Yong, T. Liu, T. Uruga, H. Tanida, D. Qi, A. Rusydi, A. T. Wee, Ti-doped ZnO thin films prepared at different ambient conditions: electronic structures and magnetic properties, *Materials* 3 (2010) 3642–3653.
- [51] D. Mardare, A. Yildiz, R. Apetrei, P. Rambu, D. Florea, N. G. Gheorghe, D. Macovei, C. M. Teodorescu, D. Luca, The Meyer-Neldel rule in amorphous TiO₂ films with different Fe content, *Journal of Materials Research* 27 (2012) 2271.

- [52] N. Jiang, D. Su, J. Spence, Determination of Ti coordination from pre-edge peaks in Ti K-edge XANES, *Physical Review B* 76 (2007) 214117.
- [53] M.-H. Tuilier, M.-J. Pac, M. Gîrleanu, G. Covarel, G. Arnold, P. Louis, C. Rousselot, A.-M. Flank, Electronic and atomic structures of $Ti_{1-x}Al_xN$ thin films related to their damage behavior, *Journal of Applied Physics* 103 (2008) 083524.
- [54] Y. Kumar, A. Tayal, W. Caliebe, M. Gupta, Study of carbon doped cobalt mononitride thin films, *Applied Surface Science* (2021) 150443.
- [55] V. Moisy-Maurice, C. De Novion, An application of Ti-K X-ray absorption edges and fine structures to the study of substoichiometric titanium carbide TiC_{1-x} , *Journal de Physique* 49 (1988) 1737–1751.
- [56] A. Longo, L. Sciortino, F. Giannici, A. Martorana, Crossing the boundary between face-centred cubic and hexagonal close packed: the structure of nanosized cobalt is unraveled by a model accounting for shape, size distribution and stacking faults, allowing simulation of XRD, XANES and EXAFS, *Journal of Applied Crystallography* 47 (2014) 1562–1568.
- [57] Seema, A. Tayal, S. Amir, S. Pütter, S. Mattauch, M. Gupta, et al., Structural, electronic, and magnetic properties of Co₄N thin films deposited using HiPIMS, *Journal of Alloys and Compounds* (2020) 158052.
- [58] M. Chassé, A. Juhin, D. Cabaret, S. Delhommaye, D. Vantelon, G. Calas, Influence of crystallographic environment on scandium K-edge X-ray absorption near-edge structure spectra, *Physical Chemistry Chemical Physics* 20 (2018) 23903–23912.
- [59] S. Chowdhury, R. Gupta, S. Prakash, L. Behera, D. Phase, M. Gupta, Study of scandium nitride thin films deposited using ion beam sputtering, in: *AIP Conference Proceedings*, volume 2265, AIP Publishing LLC, 2020, p. 030312.
- [60] M.-H. Tuilier, M.-J. Pac, G. Covarel, C. Rousselot, L. Khouchaf, Structural investigation of thin films of $Ti_{1-x}Al_xN$ ternary nitrides using Ti K-edge X-ray absorption fine structure, *Surface and Coatings Technology* 201 (2007) 4536–4541.
- [61] K. Kuriyama, Y. Takahashi, F. Sunohara, Optical band gap of Zn_3N_2 films, *Physical Review B* 48 (1993) 2781.
- [62] A. Qteish, P. Rinke, M. Scheffler, J. Neugebauer, Exact-exchange-based quasiparticle energy calculations for the band gap, effective masses, and deformation potentials of ScN, *Physical Review B* 74 (2006) 245208.
- [63] E. Burstein, Anomalous optical absorption limit in InSb, *Physical review* 93 (1954) 632.
- [64] S. Tamleh, G. Rezaei, J. Jalilian, Stress and strain effects on the electronic structure and optical properties of ScN monolayer, *Physics Letters A* 382 (2018) 339–345.
- [65] M. A. Aslam, Z. Ding, Prediction of thermodynamically stable compounds of the sc–n system under high pressure, *ACS omega* 3 (2018) 11477–11485.
- [66] J. Caicedo, G. Zambrano, W. Aperador, L. Escobar-Alarcon, E. Camps, Mechanical and electrochemical characterization of vanadium nitride (VN) thin films, *Applied Surface Science* 258 (2011) 312–320.
- [67] Q. Wu, J. Liang, J. Liu, W. Bing, X. Long, S. Luo, Characteristics of microstructure and mechanical properties of Sc films as a function of substrate temperature, *Applied surface science* 258 (2012) 7421–7424.
- [68] B. V. Sarada, C. L. Pavithra, M. Ramakrishna, T. N. Rao, G. Sundararajan, Highly (111) textured copper foils with high hardness and high electrical conductivity by pulse reverse electrodeposition, *Electrochemical and Solid State Letters* 13 (2010) D40.
- [69] P. Mayrhofer, C. Mitterer, J. Musil, Structure–property relationships in single- and dual-phase nanocrystalline hard coatings, *Surface and Coatings Technology* 174 (2003) 725–731.
- [70] H. Al-Britthen, A. R. Smith, Molecular beam epitaxial growth of atomically smooth scandium nitride films, *Applied Physics Letters* 77 (2000) 2485–2487.
- [71] P. Patsalas, C. Charitidis, S. Logothetidis, The effect of substrate temperature and biasing on the mechanical properties and structure of sputtered titanium nitride thin films, *Surface and Coatings Technology* 125 (2000) 335–340.
- [72] J. Olaya, S. Rodil, S. Muhl, L. Huerta, Influence of the energy parameter on the microstructure of chromium nitride coatings, *Surface and Coatings technology* 200 (2006) 5743–5750.
- [73] H. A. Al-Britthen, E. M. Trifan, D. C. Ingram, A. R. Smith, D. Gall, Phase stability, nitrogen vacancies, growth mode, and surface structure of ScN (001) under Sc-rich conditions, *Journal of crystal growth* 242 (2002) 345–354.
- [74] I. Schramm, M. J. Jöesaar, J. Jensen, F. Mücklich, M. Odén, Impact of nitrogen vacancies on the high temperature behavior of $(Ti_{1-x}Al_x)N_y$ alloys, *Acta Materialia* 119 (2016) 218–228.
- [75] R. Pompe, Some thermochemical properties of the system vanadium–nitrogen and vanadium–carbon–nitrogen in the temperature range 1000–1550 C, *Thermochimica Acta* 57 (1982) 273–281.
- [76] D. Gall, I. Petrov, N. Hellgren, L. Hultman, J. Sundgren, J. Greene, *Journal of Applied Physics* 84 (1998) 6034–6041.
- [77] M. A. Moram, Z. H. Barber, C. J. Humphreys, T. Joyce, P. Chalker, Young’s modulus, Poisson’s ratio, and residual stress and strain in (111)-oriented scandium nitride thin films on silicon, *Journal of Applied Physics* 100 (2006) 023514.